Piezoelectric sensitivity and hydrostatic response of novel lead-free 2–0–2 composites with two single-crystal components

V. Yu. Topolov,[a,*] C. R. Bowen,[b] A. A. Panich,[c] and A. N. Isaeva[a]

[a] *Department of Physics, Southern Federal University, 5 Zorge Street, 344090 Rostov-on-Don, Russia*

[b] *Department of Mechanical Engineering, University of Bath, Bath BA2 7AY, United Kingdom*

[c] *Institute of High Technologies and Piezotechnics, Southern Federal University, 10 Milchakov Street, 344090 Rostov-on-Don, Russia*

This paper reports the piezoelectric performance and important related hydrostatic parameters of 2–0–2 composites based on lead-free ferroelectric and piezoelectric single crystals with 4mm symmetry. We demonstrate that ferroelectric domain-engineered alkali niobate-tantalate based single crystals provide large values of the piezoelectric coefficients g_{3j}^* and related parameters when used in a 2–0–2 composite system with a relatively wide range of volume fractions of single-crystal components. An 'aspect-ratio effect' as a result of the presence of inclusions of a piezoelectric $Li_2B_4O_7$ single crystal in a polymer medium is studied for the first time for a case where the elastic compliance s_{12} in the single crystal / polymer layer of the composite passes through zero. It is observed that changes in the aspect ratio and volume fraction of the $Li_2B_4O_7$ inclusions influence the hydrostatic piezoelectric coefficient g_h^*, squared figure of merit $d_h^* g_h^*$ and electromechanical coupling factor k_h^* of the composite, and large values of $g_h^* \sim 10^2$ mV·m / N, $d_h^* g_h^* \sim (10^{-11}–10^{-10})$ Pa^{-1} and $k_h^* \approx 0.6–0.7$ are achieved. A link between $\max k_h^*$ and a change in $\mathrm{sgn}s_{12}$ is first described for the 2–2-type composite, and a comparison of the hydrostatic parameters of the novel and related composites is made. The present results show the potential of lead-free 2–0–2 composites that are suitable for piezoelectric sensor, energy-harvesting and hydroacoustic applications.

Keywords: Piezo-active composite; single crystal; piezoelectric properties; hydrostatic parameters; elastic properties

* Electronic mail: vutopolov@sfedu.ru

1. Introduction

In the last decades, piezo-active composites based on relaxor-ferroelectric single crystals (SCs), such as (1 – x)Pb($Mg_{1/3}Nb_{2/3}$)O_3 – $x$$PbTiO_3$ (PMN–xPT) and (1 – x)Pb($Zn_{1/3}Nb_{2/3}$)O_3 – $x$$PbTiO_3$ (PZN–xPT) have been developed and studied [1–3] to meet a variety of piezo-technical applications that include sensors, hydrophones, energy-harvesting devices [4, 5], etc. The overwhelming majority of SC components that exhibit outstanding electromechanical properties [6, 7] are lead-based, and there is concern that these components may pollute the environment because of the toxicity of the chemical element Pb. An important challenge in modern materials science concerned with active dielectrics and their piezo-technical applications is to find an appropriate alternative [8, 9] to lead-containing ferroelectric and piezoelectric materials, which are able to replace the well-known PZT-type ceramics [10–12] that are based on the perovskite-type Pb(Zr, Ti)O_3 solid solution.

Lead-free ferroelectric solid solutions with the perovskite-type structure are of interest due to their promising piezoelectric performance, considerable electromechanical coupling [8–11] and their potential application in a variety of transducer applications [10, 13]. For example, ferroelectric ceramics based on alkali niobates [9, 10] have become a large group of lead-free materials that are attractive due to their high piezoelectric sensitivity, large piezoelectric anisotropy, figures of merit, and high-power performance [13, 14]. Of additional interest are domain-engineered SCs based on alkali niobates-tantalates with optimised electromechanical properties. These SCs are characterised [15–17] by relatively large piezoelectric coefficients d_{ij} and electromechanical coupling factors k_{ij} (ECFs). Examples of the electromechanical properties of the [001]-poled SCs are shown in Table 1. Such SCs can be regarded as an alternative to the widespread conventional lead-containing ferroelectric ceramics, e.g., when absolute values of the piezoelectric coefficients d_{ij} are larger in the lead-free SCs in comparison to the poled polycrystalline lead-based ceramics. Another alternative is concerned with applications where there is a need for high piezoelectric sensitivity and the piezoelectric coefficient g_{33} of the SCs is large in comparison to the moderate values of g_{33} of many poled polycrystalline ceramics. In addition to replacing lead-based bulk materials, new examples of high-performance piezoelectrics can be achieved by using the lead-free SCs as components in modern piezo-active composite configurations [18, 19] with 1–3 and 2–2 connectivity patterns.

In recent work [20], a laminar three-component SC / ceramic / polymer composite, which was based on the [001]-poled PMN–0.33PT SC and described by 2–0–2 connectivity in terms of Refs. 4, 21, was found to exhibit a large hydrostatic piezoelectric response. In earlier experimental studies [22], a promising example of a 2–0–2 composite based on a ferroelectric ceramic was demonstrated, and the improved piezoelectric performance of this composite was shown to be a result of an active role of lead-free inclusions present in the polymer layers. However the role of the heterogeneous layer and its active component has yet to be studied in detail. The aim of

the present paper is to analyse the piezoelectric performance and hydrostatic parameters of the 2–0–2 composites based on the [001]-poled lead-free SCs and to demonstrate the potential of these novel lead-free composite materials in comparison to the 2–2-type lead-containing composites.

2. Model of the 2–0–2 composite, its effective parameters and components

2.1. Model of the composite

The 2–0–2 composite consists of a system of parallel-connected layers of two types (*Type I* and *Type II* layers, Fig. 1) with interfaces that are parallel to the (X_2OX_3) plane. These layers are regularly arranged along the coordinate OX_1 axis. The Type I layer is a ferroelectric domain-engineered SC and is characterised by a spontaneous polarisation $\boldsymbol{P}_s^{(1)}$ and volume fraction m. Hereafter we denote this component *SC-1*. Its main crystallographic axes X, Y and Z are oriented as follows: $X \parallel [001] \parallel OX_1$, $Y \parallel [010] \parallel OX_2$ and $Z \parallel [001] \parallel OX_3$, where the [*hkl*] direction is given in the perovskite unit-cell axes. The orientation of the non-180° domains formed in the ferroelectric 3*m* phase under an electric field $\boldsymbol{E} \parallel OX_3$ is shown in the inset 1 in Fig. 1. At equal volume fractions of these domains, the SC-1 is characterised by 4*mm* symmetry [6, 7, 15–17].

The Type II layer is a SC-2 / polymer medium with 0–3 connectivity in terms of Ref. 21, and the volume fraction of the Type II layers is $1 - m$ (Fig. 1). The shape of each SC-2 inclusion is shown in the inset 2 in Fig. 1 and obeys the equation $(x_1 / a_1)^2 + (x_2 / a_2)^2 + (x_3 / a_3)^2 = 1$ in the co-ordinate OX_f axes. Hereby $\rho_i = a_1 / a_3$ is the aspect ratio of the SC-2 inclusion, and m_i is the volume fraction of the SC-2 in the Type II layer. We assume that the linear sizes of each SC-2 inclusion are much smaller than the thickness of each layer of the composite sample shown in Fig. 1. The SC-2 inclusions occupy sites of a simple tetragonal lattice with unit-cell vectors parallel to the OX_f axes. As with the SC-1, the orientation of the crystallographic axes X, Y and Z of each SC-2 inclusion in the Type II layer is given by $X \parallel OX_1$, $Y \parallel OX_2$ and $Z \parallel OX_3$.

2.2. Effective properties and hydrostatic parameters of the composite

Effective electromechanical properties of the 2–0–2 composite are evaluated in two stages which will now be described. During the first stage, we calculate the effective electromechanical properties of the Type II layer by regarding it as a 0–3 SC-2 / polymer composite. These effective properties are determined by means of the effective field method [4] that takes into consideration an interaction between the SC-2 inclusions. We assume that the components in the Type II layer are characterised by elastic moduli $c_{ab}^{(SC),E}$ (SC-2) and $c_{ab}^{(p),E}$ (polymer), piezoelectric coefficients $e_{ij}^{(SC)}$ (SC-2) and $e_{ij}^{(p)}$ (polymer), and dielectric permittivities $\varepsilon_{qq}^{(SC),\xi}$ (SC-2) and $\varepsilon_{qq}^{(p),\xi}$ (polymer), where the superscript E denotes measurements at E = const, and the superscript ξ denotes

measurements at the constant strain. The effective electromechanical properties of the Type II layer are represented in the form of the 9×9 matrix as follows:

$$|| C^{(2)} || = \begin{pmatrix} || c^{(2),E} || & || e^{(2)} ||^t \\ || e^{(2)} || & - || \varepsilon^{(2),\xi} || \end{pmatrix}. \quad (1)$$

In Eq. (1), the superscript t denotes the transposition. Elements of $|| C^{(2)} ||$ are calculated using the formula [4] within the framework of the effective field medium

$$|| C^{(2)} || = || C^{(p)} || + m_i (|| C^{(SC)} || - || C^{(p)} ||)[|| I || + (1 - m_i)|| S ||\cdot|| C^{(p)} ||^{-1}(|| C^{(SC)} || - || C^{(p)} ||)]^{-1}. \quad (2)$$

In Eq. (2), $|| C^{(SC)} ||$ and $|| C^{(p)} ||$ are matrices of the properties of SC-2 and polymer, respectively, m_i is the volume fraction of the SC-2 component in the Type II layer, $|| I ||$ is the identity matrix, and $|| S ||$ is the matrix that contains the Eshelby tensor components [23]. The matrix $|| S ||$ depends on elements of $|| C^{(p)} ||$ and the aspect ratio ρ_i of the SC-2 inclusion. The matrices $|| C^{(SC)} ||$ and $|| C^{(p)} ||$ from Eq. (2) have the form similar to that shown in Eq. (1).

During the second stage, the effective electromechanical properties of the 2–0–2 composite system as a whole are calculated using the matrix method [4, 20] that allows for the electromechanical interaction between the Type I and Type II layers shown in Fig. 1. The electromechanical properties of the Type I and Type II layers are described by a 9×9 matrix

$$|| C^{(n)} || = \begin{pmatrix} || s^{(n),E} || & || d^{(n)} ||^t \\ || d^{(n)} || & || \varepsilon^{(n),\sigma} || \end{pmatrix}. \quad (3)$$

In Eq. (3), $|| s^{(n),E} ||$ is the 6×6 matrix of elastic compliances at E = const, $|| d^{(n)} ||$ is the 3×6 matrix of piezoelectric coefficients, $|| \varepsilon^{(n),\sigma} ||$ is the 3×3 matrix of dielectric permittivities of the Type I layer (n = 1) and Type II layer (n = 2), the superscript σ denotes measurements at constant stress, and the superscript t denotes the transposition. A transition from the matrix elements of the Type II layer in the form of Eq. (2) to the matrix elements in the form of Eq. (3) is carried out using conventional formulae [24] for the piezoelectric medium. The matrix of the effective electromechanical properties of the 2–0–2 composite is represented [20] as

$$|| C^* || = [|| C^{(1)} ||\cdot|| M || m + || C^{(2)} || (1 - m)] [|| M || m + || I || (1 - m)]^{-1} \quad (4)$$

and has the structure shown in Eq. (3). In Eq. (4), $|| C^{(1)} ||$ and $|| C^{(2)} ||$ are taken from Eq. (3), $|| M ||$ is concerned with boundary conditions at the interface x_1 = const (Fig. 1), and $|| I ||$ is the identity matrix. The boundary conditions [4] at $x_1 =$ const imply a continuity of components of mechanical stress σ_{11}, σ_{12} and σ_{13}, strain ξ_{22}, ξ_{23} and ξ_{33}, electric displacement D_1, and electric field E_2 and E_3.

Hereafter we consider $|| C^* ||$ from Eq. (4) as a function of three variables, i.e., $|| C^* || = || C^*(m, \rho_i, m_i) ||$. Based on the matrix elements of $|| C^* ||$ from Eq. (4), we find the piezoelectric coefficients g_{ij}^* by using the relation [4,

24] $\| g^* \| = \| \varepsilon^{*\sigma} \|^{-1} \cdot \| d^* \|$. In the present paper we analyse the following effective parameters of the 2–0–2 composite:

(i) the piezoelectric coefficients g_{3j}^* and squared figure of merit associated with the longitudinal piezoelectric effect

$$(Q_{33}^*)^2 = d_{33}^* g_{33}^*, \tag{5}$$

(ii) the hydrostatic piezoelectric coefficient

$$g_h^* = g_{33}^* + g_{32}^* + g_{31}^*, \tag{6}$$

(iii) the hydrostatic squared figure of merit

$$(Q_h^*)^2 = d_h^* g_h^*, \tag{7}$$

and

(iv) the hydrostatic ECF

$$k_h^* = d_h^* / (\varepsilon_{33}^{*\sigma} s_h^{*E})^{1/2}. \tag{8}$$

In Eq. (7), $d_h^* = d_{31}^* + d_{32}^* + d_{33}^*$ is the hydrostatic piezoelectric coefficient, and in Eq. (8),

$$s_h^{*E} = \sum_{a=1}^{3} \sum_{b=1}^{3} s_{ab}^{*E} \tag{9}$$

is the hydrostatic elastic compliance at $E = \text{const}$. Eqs. (5) – (8) are written for the case when the electrodes, that are applied to the composite (Fig. 1), are parallel to the (X_1OX_2) plane. The piezoelectric coefficients g_{3j}^* are used to describe the piezoelectric sensitivity in specific directions for an external force applied to the sample. The squared figure of merit $(Q_{33}^*)^2$ from Eq. (5) is used to evaluate the sensor signal-to-noise ratio due to the longitudinal piezoelectric effect [4]. When the composite sample is under hydrostatic loading, the hydrostatic piezoelectric coefficient g_h^* describes the piezoelectric sensitivity, the squared figure of merit $(Q_h^*)^2$ from Eq. (7) is concerned with the sensor signal-to-noise ratio, and the ECF k_h^* from Eq. (8) characterises the effectiveness of the energy conversion [4] from the mechanical form into the electric form and vice versa. Taking into account the piezoelectric items from Eq. (6), we study the piezoelectric anisotropy of the composite.

2.3. Lead-free components of the composite

Among the lead-free components of interest for our further analysis, we consider the ferroelectric [001]-poled SCs (Table 1) in the Type I layer, a piezoelectric $Li_2B_4O_7$ (LBO) SC as an inclusion material in the polymer medium in the Type II layer, and monolithic polyethylene (PE) and polyurethane as matrix materials in the Type II layer. The properties of the components related to the Type II layer are shown in Table 2. It should be noted that the LBO SC is

a highly original component to use in a composite for the following reasons. First, the symmetry of the LBO SC in the Type II layer coincides with the macroscopic symmetry of the [001]-poled SC in the Type I layer. Second, the signs of the piezoelectric coefficients e_{ij} of the LBO SC (see Table 2) coincide with the signs of e_{ij} of the highly anisotropic $PbTiO_3$-type ceramics [12, 29], however the piezoelectric effect in the LBO SC is weaker than that in the poled $PbTiO_3$-type ceramics. Third, the LBO SC is characterised by a considerable elastic anisotropy (Table 2), and the large ratio $c_{13}^E / c_{12}^E \approx 9.4$ has no analogies with other ferroelectric ceramics and SCs. The [001]-poled SCs listed in Table 1 are of additional interest because they exhibit a high piezoelectric sensitivity. For instance, the piezoelectric coefficient g_{33} (in mV·m / N) is 68.6, 50.6 and 94.7 for the KNN–T, KNN–TL and KNNTL:Mn SC, respectively. It is worth highlighting some lead-containing materials as a comparison. For example, the [001]-poled PMN–0.33PT SC [30] has a very high piezoelectric activity (d_{33} = 2820 pC /N) and is characterised by a lower piezoelectric coefficient g_{33} of 38.9 in mV·m / N, and a poled modified $PbTiO_3$ ceramic [29] with d_{33} = 53 pC / N is characterised by a g_{33} = 33.3 mV·m / N and $g_{33} / |g_{31}| >> 1$. We note that the piezoelectric coefficient d_{33} of the [001]-poled KNNTL:Mn SC (see Table 1) is about 10 times larger than d_{33} of the aforementioned modified $PbTiO_3$ ceramic from work [29].

In the presence of the two SC components, that belong to the 4*mm* symmetry class, and an isotropic polymer component, the 2–0–2 composite shown in Fig. 1 is described by *mm*2 symmetry. For this symmetry class [4, 24], relations between the piezoelectric coefficients

$$g_{3j}^* = d_{3j}^* / \varepsilon_{33}^{*\sigma} \text{ and } g_h^* = d_h^* / \varepsilon_{33}^{*\sigma} \quad (10)$$

hold, where j = 1, 2 and 3.

3. Piezoelectric sensitivity and hydrostatic parameters of the 2–0–2 composite

In Section 3 we discuss the behaviour of the piezoelectric coefficients g_{3j}^* from Eqs. (6) and (10) as well as features of the piezoelectric sensitivity and hydrostatic parameters of the 2–0–2 composite shown in Fig. 1. We consider the piezoelectric performance of the 2–0–2 composite based on the domain-engineered KNNTL:Mn SC that exhibits the largest piezoelectric coefficients d_{33} and g_{33} among the ferroelectric SCs listed in Table 1.

3.1. The 'aspect-ratio' effect

It is assumed that the volume fraction of the SC-2 is m_i = const in the Type II layer (see the inset 2 in Fig. 1), and the aspect ratio $0.01 \le \rho_i \le 100$ is varied to tailor the elastic anisotropy of the Type II layer. We remind the reader that the aspect ratios $\rho_i < 1$ are related to prolate inclusions, $\rho_i = 1$ is related to spherical inclusions, and $\rho_i > 1$ are

related to oblate inclusions. The data in Table 3 suggests that the elastic compliances $s_{ab}^{(2),E}$ of the Type II layer (i.e., 0–3 LBO SC / PE composite) undergo considerable changes on varying ρ_i in a wide range of volume fractions where $m_i \leq 0.2$. In Table 3 we do not show the shear elastic compliances $s_{44}^{(2),E}$ and $s_{66}^{(2),E}$ because of their negligible influence on the longitudinal and transverse piezoelectric effects in the composite of Fig. 1. The Type II layer at $\rho_i >> 1$ is characterised by effective properties that obey the conditions $|d_{3j}^{(2)}| << |d_{3j}^{(1)}|$ and $\varepsilon_{pp}^{(2),\sigma} << \varepsilon_{pp}^{(1),\sigma}$. The elastic compliances $s_{11}^{(2),E}$ and $s_{33}^{(2),E}$ at $\rho_i >> 1$ become comparable to $s_{11}^{(1),E}$ and $s_{33}^{(1),E}$, respectively, however differences between $s_{1b}^{(2),E}$ and $s_{1b}^{(1),E}$ ($b = 2$ and 3) remain large. Moreover, we observe a sign-variable behaviour of $s_{12}^{(2),E}$, i.e., the condition

$$s_{12}^{(2),E} = 0 \tag{11}$$

is achieved at $\rho_i > 10$ and $m_i > 0.1$ (see the 7th column in Table 3). This unusual contrast between the elastic properties of the Type I and Type II layers leads to an improvement of the hydrostatic piezoelectric parameters of the composite when the aspect ratio ρ_i of the SC-2 inclusions is increased. This improvement is due a reduction in the transverse piezoelectric activity of the composite at $\rho_i >> 1$, which leads to a decrease in $|d_{3b}^*|$ and an increase in d_h^*. It should be added that similar changes in the elastic properties and validity of Eq. (11) are observed if we replace the PE matrix with a higher stiffness polyurethane matrix in the Type II layer. This indicates that the LBO SC, with its unique elastic anisotropy (see data in Table 2), influences the elastic properties of the Type II layer for a range of ρ_i values, and this influence can be of value for improving the composite performance for specific applications.

The graphs in Fig. 2 suggest that the effect of aspect-ratio is appreciable, even at relatively small volume fractions of SC-1 ($m \leq 0.2$) and SC-2 ($m_i = 0.1$). The small values of m and m_i enable the composite to achieve large absolute values of g_{3j}^*, see Fig. 2a–c. A non-monotonic dependence of g_{3j}^* on the aspect ratio ρ_i is observed in Fig. 2a–c at $0 < \rho_i < 3$, i.e., in the region where the elastic compliances of the Type II layer $s_{ab}^{(2),E}$ undergo large changes, see Table 3. On comparing Fig. 2a and Fig. 2b, we see differences between $\min g_{31}^*$ and $\min g_{32}^*$. The interfaces $x_1 = \text{const}$ in the composite, as seen in Fig. 1, influence the piezoelectric effect concerned with g_{31}^* to a larger extent in comparison to the piezoelectric effect concerned with g_{32}^*. As a consequence, the depth of $\min g_{31}^*$ is larger than that of $\min g_{32}^*$ (cf. Fig. 2a and 2b), however values of $|g_{31}^*|$ near $\min g_{31}^*$ are smaller than values of $|g_{32}^*|$ near $\min g_{32}^*$. As for the piezoelectric coefficient g_{33}^*, its aspect-ratio dependence shown in Fig. 2c is

characterised by a diffuse maximum that correlates with $\max s_{33}^{(2),E}$ of the Type II layer, see the 5th column in Table 3.

The sequence of the curves 1–4 in all of the graphs in Fig. 2 is related to the strong influence of the SC-1 component in the Type I layer on the piezoelectric sensitivity and other parameters of the composite: it is seen that on increasing the volume fraction m of the SC-1, the effective parameters $|g_{3j}^*|$, $(Q_{33}^*)^2$ etc. decrease at ρ_i = const and m_i = const. This occurs mainly because of the large dielectric permittivity $\varepsilon_{33}^{(1),\sigma}$ of the SC-1 in comparison to $\varepsilon_{33}^{(2),\sigma}$ of the Type II layer. It should be added that the aspect-ratio dependence of the effective parameters in Fig. 2 remains similar when PE is replaced with polyurethane in the Type II layer.

We can observe that the squared figure of merit $(Q_{33}^*)^2$ in Fig. 2d undergoes changes which are similar to those of g_{33}^* in Fig. 2c at m_i = const and m = const. This means that the influence of the piezoelectric coefficient d_{33}^* on $(Q_{33}^*)^2$ from Eq. (5) is small due to the relatively small volume fractions m_i and m. Taking into account Eqs. (10), we can represent the link in Eq. (5) as follows:

$$(Q_{33}^*)^2 = (g_{33}^*)^2 \varepsilon_{33}^{*\sigma}. \tag{12}$$

Changes in $\varepsilon_{33}^{*\sigma}$ of the composite with the aspect ratio ρ_i at m_i = const and m = const are minor because of minor changes in $\varepsilon_{33}^{(2),\sigma}$ of the Type II layer in a wide range of ρ_i. On comparing graphs in Fig. 2c and Fig. 2e, we see that the piezoelectric coefficient g_{33}^* plays a key role in forming the aspect-ratio dependence of the hydrostatic piezoelectric coefficient g_h^* from Eq. (6). At $\rho_i >> 1$ the role of the contributions from $g_{31}^* < 0$ and $g_{32}^* < 0$ to g_h^* weakens, and this leads to increasing g_h^* values on increasing ρ_i, see Fig. 2e. The similarity of the shape of the graphs in Fig. 2e and 2f is a result of the strong influence of the hydrostatic piezoelectric coefficient g_h^* on the squared figure of merit $(Q_h^*)^2$ from Eq. (7). Taking into account Eqs. (10), we write $(Q_h^*)^2$ by analogy with Eq. (12) as follows:

$$(Q_h^*)^2 = (g_h^*)^2 \varepsilon_{33}^{*\sigma}. \tag{13}$$

Due to the minor changes in $\varepsilon_{33}^{*\sigma}$ of the composite at m_i = const and m = const, the important influence of $(g_h^*)^2$ on the $(Q_h^*)^2$ parameter is clear in accordance with Eq. (13).

Of specific interest is the aspect-ratio dependence of the hydrostatic ECF k_h^*, see Fig. 2g. Taking into account Eqs. (7), (8) and (13), we represent $(k_h^*)^2$ as

$$(k_h^*)^2 = (Q_h^*)^2 / s_h^{*E}. \tag{14}$$

Our analysis of the hydrostatic elastic compliance s_h^{*E} from Eq. (9) at $m_i = 0.1$ and $0.05 \le m \le 0.20$ shows that s_{33}^{*E} provides a considerable contribution to s_h^{*E}, and $s_{33}^{(2),E}$ has a strong influence on the s_{33}^{*E} value. This influence is associated with the microgeometry of the Type II layer (see the inset 2 in Fig. 1) and the small volume fractions m_i and m reported above mean that the polymer component plays a dominant role in the overall response and effective properties of the composite. Changes in $s_{33}^{(2),E}$ on varying the aspect ratio ρ_i in the Type II layer are not significant (see, for instance, the 5th column in Table 3) and, therefore, do not lead to appreciable changes in s_h^{*E}. This circumstance and Eq. (14) can explain the similar aspect-ratio dependences of $(k_h^*)^2$ and $(Q_h^*)^2$ in Fig. 2f and g.

3.2. Non-monotonic volume-fraction dependences

The data from Fig. 2e–g show that the largest values of the composite hydrostatic parameters at m_i = const and m = const are achieved at $\rho_i = 100$, i.e., when highly oblate SC-2 inclusions are present in the Type II layer. The graphs in Fig. 3 show that the volume-fraction (m and m_i) dependence of the effective parameters of the composites when the polymer component is either PE (Fig. 3a–d) or polyurethane (Fig. 3e and f); in both cases the aspect ratio is $\rho_i = 100$. It can be seen from our data for the 2–0–2 composites that the local max g_{33}^* and max g_h^* are achieved [20] at small volume fractions of SC-1 ($0 < m < 0.03$); see, for instance, Fig. 3a, b and e. The small m values highlight that the dielectric properties of the composite play an important role in forming max g_{33}^* and max g_h^*. In a similar way to the parallel-connected 2–2 SC / polymer [3, 4] and ferroelectric ceramic / polymer [31] composites, max g_{33}^* and max g_h^* are achieved at $m << 1$ due to the rapid increase of d_{33}^* and d_h^* and a relatively slow increase of $\varepsilon_{33}^{*\sigma}$.

Changes in the volume fraction m_i of SC-2 do not lead to large changes in the g_{33}^* and g_h^* curves in Fig. 3a, b and e because of the small dielectric permittivity of the Type II layer, i.e., the condition $\varepsilon_{33}^{(1),\sigma} << \varepsilon_{33}^{(2),\sigma}$ holds. It can be seen from Fig. 3b that changes in the volume fraction m_i lead to a non-monotonic dependence of g_h^* at m = const. This is a result of changes in contributions from the piezoelectric coefficients g_{3j}^* of the composite into g_h^* from Eq. (6).

We now consider the volume fraction of SC-1 $m = 0.10$ as an example to demonstrate the high level of the piezoelectric sensitivity in this particular composite system: from the data in Fig. 3, a, b and e, values of $g_{33}^* \sim (10^2 - 10^3)$ mV·m / N and $g_h^* \sim 10^2$ mV·m / N are achieved. On comparing the graphs in Fig. 3a and 3e, we see that the

piezoelectric coefficient g_{33}^{*} is smaller at m = const and m_i = const for the polyurethane-containing composite. The polymer matrix with the larger elastic moduli c_{ab} (see Table 2) leads to a stiffer Type II layer which leads to a decrease in the overall piezoelectric sensitivity of the composite.

The similarity of graphs in Fig. 3b and 3c is a result of the contribution of the hydrostatic piezoelectric coefficient g_h^{*} to the squared figure of merit $(Q_h^{*})^2$, which originates from Eq. (13). In the volume-fraction ranges shown in Fig. 3b and 3c, the dielectric permittivity $\varepsilon_{33}^{*\sigma}$ of the composite slowly increases with increasing m at m_i = const and, therefore, does not strongly affect the volume-fraction dependence of $(Q_h^{*})^2$. A comparison of graphs in Fig. 3d and 3f for the PE-containing and polyurethane-containing composite, respectively, suggests that the value and location of absolute max k_h^{*} depend on the polymer component. In the case of a composite based on the softer PE polymer, the value of absolute max k_h^{*} is approximately 20% larger than in the composite with the higher stiffness polymer (polyurethane). Moreover, the elastic properties of the polymer influence the volume fraction m_i that is related to absolute max k_h^{*}. This influence is due to the active role of the Type II layer in forming max k_h^{*} since it can be seen from Fig. 3d and 3f that local max $k_h^{*} = (k_h^{*})_m$ is observed at $m < 0.2$, i.e., at large volume fractions of the Type II layer. Changes in the volume fraction of SC-2 m_i lead to changes in the piezoelectric coefficients of the Type II layer and, therefore, to changes in the piezoelectric properties, electromechanical coupling and hydrostatic parameters of the composite.

By analysing the volume-fraction behaviour of the hydrostatic ECF k_h^{*} by using Eq. (14), one can highlight the important role of the hydrostatic compliance s_h^{*E} on the electromechanical coupling. At volume fractions $m <$ 0.2, where $(k_h^{*})_m$ is achieved, one can assume that $s_h^{*E} \approx s_h^{(2),E}$ because of large values of the elastic compliances of the Type II layer. Among the elastic compliances $s_{ab}^{(2),E}$ that contribute to $s_h^{(2),E}$, of particular interest is $s_{12}^{(2),E}$ that is close to zero (see, for instance, the 7th column of Table 3). In the case of $\rho_i = 100$, we find a link between the local maximum of k_h^{*} of the composite, $(k_h^{*})_m$, and the sign-variable behaviour of the elastic compliance $s_{12}^{(2),E}$ of the Type II layer; see Fig. 4a where $s_{12}^{(2),E} \to 0$. The graph in Fig. 4a is built using the k_h^{*} values related to $(k_h^{*})_m$ at m_i = const. Fig. 4b shows a relation between the SC-1 volume fraction m_{maxkh}, at which $(k_h^{*})_m$ appears, and the SC-2 volume fraction m_i. It is seen that changes in m_i lead to only small changes in m_{maxkh}. In Fig. 4c we show the volume-fraction (m_i) behaviour of the electromechanical properties from Eq. (8), and these properties are calculated for the composite at $m = m_{maxkh}$. In the vicinity of absolute max k_h^{*}, the hydrostatic elastic compliance

s_h^{*E} undergoes the largest changes, see curve 1 in Fig. 4c. In our opinion, such a performance of the composite can be of value at further predictions of the hydrostatic piezoelectric response.

3.3. Achieving a large piezoelectric anisotropy

The large contribution from the piezoelectric coefficient g_{33}^* (Figs. 2c and 3a) to the hydrostatic coefficient g_h^* (see Figs. 2d and 3b) is a stimulus for a further analysis of a large piezoelectric anisotropy in the 2–0–2 composite. This problem is of independent interest due to the potential of these materials for piezoelectric energy-harvesting applications [4]. There are various modified $PbTiO_3$ ceramic compositions [12, 29] that are characterised by a large anisotropy of their piezoelectric coefficients d_{3j} or g_{3j}: for these materials in the poled state, the condition $d_{33}/|d_{31}| = g_{33}/|g_{31}| >> 1$ holds. Recently, a 2–0–2 composite[20] that contains the SC, ceramic and polymer components was studied, however the modified $PbTiO_3$ ceramic inclusions in the polymer matrix were assumed to be non-poled.

For the 2–0–2 studied PE-containing composite, the condition

$$g_{33}^*/|g_{3f}^*| = d_{33}^*/|d_{3f}^*| \geq 5 \qquad (15)$$

holds at $\rho_i >> 1$, where $f = 1$ and 2. This circumstance is due to the to the active role of the Type II layer in forming the piezoelectric response along the OX_1 and OX_2 axes. For example, according to Table 3, the Type II layer at $\rho_i = 100$ is characterised by an elastic compliance $s_{33}^{(2),E}$ that is a few times larger than $s_{11}^{(2),E}$, and a large difference between $s_{12}^{(2),E}$ and $s_{13}^{(2),E}$ is observed. The volume fraction m of the SC-1 strongly depends on the volume fraction m_i of the SC-2. We see that the volume fractions m that obey the condition (15) are located in a relatively narrow range of less than 0.25 (the shaded region in Fig. 5), while m_i can be taken from a wide range (0.05 to 0.75). The volume fraction $0 < m < 0.25$ indicates that the Type I layer plays a 'modest role' in forming the large piezoelectric anisotropy of the composite, while the volume fraction of the Type II layer is more influential, and its electromechanical properties and anisotropy can be varied due to the wide m_i and ρ_i ranges.

The next example of the piezoelectric performance at the condition (15) is concerned with the 2–0–2 KNNTL:Mn SC / LBO SC / PE composite at $m_i = 0.50$ and $\rho_i = 100$. In a case of the volume fraction $m = 0.20$, such a composite is characterised by $g_{33}^* = 432$ mV·m / N, $g_h^* = 288$ mV·m / N, $(Q_{33}^*)^2 = 136 \cdot 10^{-12}$ Pa^{-1}, $(Q_h^*)^2 = 60.5 \cdot 10^{-12}$ Pa^{-1}, and $k_h^* = 0.674$. At the volume fraction $m = 0.10$, we obtain $g_{33}^* = 774$ mV·m / N, $g_h^* = 614$ mV·m / N, $(Q_{33}^*)^2 = 188 \cdot 10^{-12}$ Pa^{-1}, $(Q_h^*)^2 = 119 \cdot 10^{-12}$ Pa^{-1}, and $k_h^* = 0.709$. The set of the effective parameters presented above is a result of a decrease of the dielectric permittivity $\varepsilon_{33}^{*\sigma}$ of the composite on decreasing the volume fraction

m of SC-1. We mention that $\varepsilon_{33}^{*\sigma}$ is linked to these effective parameters in accordance with Eqs. (8), (10, (12), and (13).

It should be added that the condition (15) is also valid at volume fractions m and m_i which are related to absolute max k_h^* of the same 2–0–2 composite at ρ_i = 100 (see Fig. 4a and b). This is consistent with the result [32] that max k_h^* of the 2–2-type composite correlates with max d_h^*, and the validity of condition (15) undoubtedly facilitates the achievement of large values of d_h^*. As follows from our data for the composite at ρ_i = 100, the absolute max k_h^* = 0.714 (see Figs. 3d and 4a) is achieved at volume fractions m_i = 0.61 and m_{maxkh} = 0.126 (see Fig. 4b). At these volume fractions, the piezoelectric coefficients of the composite would be d_h^* = 189 pC / N and d_{33}^* = 244 pC / N. The maximum value of d_h^* at ρ_i = 100 and m_i = 0.61 is equal to 201 pC / N and achieved at m_{maxdh} = 0.210, i.e., the relatively small difference $m_{maxdh} - m_{maxkh} \approx 0.08$ is present.

Thus, our results suggest that the combination of the following factors is favourable to achieve the high hydrostatic performance of the studied 2–0–2 composite: (i) the use of a SC-1 component with a large g_{33} and relatively large d_{33} value, (ii) the use of SC-2 component with remarkable anisotropy of the piezoelectric and elastic properties (see Table 2), (iii) using oblate shaped SC-2 inclusions aligned in the Type II layer (see the inset 2 in Fig. 1), and (iv) using a relatively soft polymer component in comparison to both SC components of the composite. The symmetry of the SC components influences the piezoelectric response of the composite to a certain degree, and the coincidence of the symmetry classes of the SC-1 and SC-2 facilitates the prediction of the hydrostatic response and parameters from Eqs. (6)–(8).

4. Comparison of effective parameters

4.1. Influence of SC in the Type I layer on maxima of effective parameters

In Table 1 we have given the full sets of electromechanical constants of three lead-free ferroelectric SCs, however in previous sections we have analysed the performance of the 2–0–2 composites based on the KNNTL:Mn SC only. In our opinion, the KNN–T and KNN–TL SCs listed in Table 1 are less effective as piezoelectric components of the 2–0–2 composites since the piezoelectric coefficients d_{33} and elastic compliances $|s_{fj}^E|$ of these SCs at f, j = 1, 2 and 3 are smaller than the related constants of the KNNTL:Mn SC. Data from Table 4 show that maximum values of the effective parameters (5) and (7) of the composites based on KNN–T and KNN–TL SCs are much smaller than the maximum values of the same parameters of the composite based on the KNNTL:Mn SC (see Figs. 2d, f and 3c, d). In addition, only the hydrostatic ECF k_h^* from Eq. (8) can compete

with the local max k_h^* values of the KNNTL:Mn SC / LBO SC / polyurethane composite (Fig. 3f): as seen from Table 4, at m_i = 0.50, we have $0.5 < \max k_h^* < 0.6$ and minor changes on replacing the KNN–T SC with the KNN–TL SC in the composite. Such a feature can be concerned with the active role of the Type II layer in forming the hydrostatic electromechanical coupling at $0.05 < m < 0.1$, in the vicinity of local max k_h^*. Moreover, the elastic anisotropy of the Type II layer promotes a weakening of the transverse piezoelectric effect in the composite and, therefore, increasing d_h^* and k_h^*.

We add that the condition (15) holds for the KNN–T- and KNN–TL-based composites from Table 4 at volume fractions m related to local max k_h^* at m_i = 0.30 and 0.50. However the volume-fraction (m) range of validity of the condition (15) is narrower than in the case of the KNNTL:Mn-based composite (Fig. 5). For instance, the range of validity of the condition (15) is $0.001 \le m \le 0.071$ (at m_i = 0.30) or $0.001 \le m \le 0.135$ (at m_i = 0.50) for the KNN–T-based composite, and this range is $0.001 \le m \le 0.101$ (at m_i = 0.30) or $0.001 \le m \le 0.185$ (at m_i = 0.50) for the KNN–TL-based composite. At m = 0.10 and m_i = 0.50, the piezoelectric coefficient associated with the longitudinal sensitivity equals g_{33}^* = 543 mV·m / N (KNN–T-based composite) or 402 mV·m / N (KNN–TL-based composite), and these values are smaller than g_{33}^* = 774 mV·m / N related to the KNNTL:Mn-based composite at the same set of m, m_i and ρ_i.

4.2. Comparison to related ferroelectric materials

The studied 2–0–2 lead-free composites have advantages over various ferroelectric ceramics and composites. For instance, a ferroelectric nanostructured Mn-modified $(K_{0.5}Na_{0.5})NbO_3$ polycrystalline ceramic is characterised [14] by piezoelectric coefficients d_{33} = 340 pC / N and g_{33} = 220 mV·m / N, squared figure of merit $(Q_{33})^2$ = $74.8 \cdot 10^{-12}$ Pa^{-1}, and the piezoelectric anisotropy factor $d_{33} / |d_{31}| \approx 21$. The piezoelectric coefficient d_{33} of the Mn-modified $(K_{0.5}Na_{0.5})NbO_3$ is therefore comparable to d_{33}^* of the 2–0–2 composites, however the g_{33}^* and $(Q_{33}^*)^2$ value of the ceramic are smaller than the composite (see data in Figs. 2c, d and 3a, e and Table 4). Very recently, a grain-oriented and highly textured modified $PbTiO_3$ material has been manufactured, with a reported value[33] of g_{33} = 115 mV·m / N which is smaller than g_{33}^* of the studied 2–0–2 lead-free composites.

According to reported data [31] on a 2–2 PZT ceramic / polymer composite, its max g_h^* = 310 mV·m / N is achieved at a volume fraction of ceramic $0 < m_{cer} < 0.01$. At m_{cer} = 0.1, the 2–2 composite is characterised[31] by g_h^* = 39.4 mV·m / N and $(Q_h^*)^2 = 2.34 \cdot 10^{-12}$ Pa^{-1}. Therefore, despite the comparable piezoelectric coefficient d_{33} of PZT ceramics [12] with the lead-free SCs in Table 1, the effective parameters g_h^* and $(Q_h^*)^2$ of the 2–2 PZT-based

composite are smaller than those related to the 2–0–2 lead-free composites. The g_{33}^* and g_h^* values of the 2–0–2 composite at m = 0.1 (see Figs. 2c, e and 3a, b, e) and the g_{33}^* and g_h^* values related to a 2–2 $KNbO_3$ SC / polyurethane composite [19] at m = 0.1 have equal orders-of-magnitude. However on increasing the volume fraction m of the $KNbO_3$ SC in the 2–2 composite, both its g_{33}^* and g_h^* decrease more intensively [19] than the 2–0–2 composite studied here. We add that for the 2–2 composite based on single-domain $KNbO_3$ SC [34] from the *mm*2 symmetry class, the polarisation orientation effect was studied [19] to improve the piezoelectric sensitivity and examine conditions for the large piezoelectric anisotropy.

For a 2–2 composite based on the [011]-poled PMN–*x*PT SC [6], a value of $(Q_h^*)^2 = 1.6 \cdot 10^{-11}$ Pa^{-1} is smaller than $(Q_h^*)^2$ of the 2–0–2 composites studied in this work (see Figs. 2f and 3c) despite a high piezoelectric activity of the lead-containing SC component [3, 4]. This is due to the smaller influence of the polymer component and the composite architecture on the hydrostatic piezoelectric response in the 2–2 SC / polymer composite. The values of $(Q_h^*)^2 \approx 10^{-10}$ Pa^{-1} related to the 2–0–2 composite studied in this work (see data in Fig. 2f) are approximately seven times larger than the $(Q_h^*)^2$ of oriented PZT ceramic / polymer composites [35] with 2–2 connectivity patterns and two times larger than the $(Q_h^*)^2$ value of oriented 3–3 PZT ceramic / polymer composites [35].

In Table 5 we compare the hydrostatic parameters of the 2–0–2 composites based on the [001]-poled SCs. The PMN–0.33PT- and PZN–0.08PT-based composites with 2–0–2 connectivity were studied in work [20]. We choose the aspect ratio ρ_i = 100 at which the largest hydrostatic parameters are expected, see for instance, Fig. 2e–g. The lead-free composite based on the KNNTL:Mn SC demonstrates advantages over the two lead-containing composites from work [20] due to large values of the piezoelectric coefficient g_h^* from Eqs. (6) and (10), see data in the 3rd, 5th and 7th columns of Table 5. The larger piezoelectric coefficient g_h^* is achieved in the KNNTL:Mn –based composite because of its moderate dielectric permittivity in comparison to the lead-containing composites from work [20]. However in the represented range of volume fractions m and m_i, the hydrostatic ECF k_h^* from Eq. (8) is larger in the lead-containing composites, see the 6th and 8th columns of Table 5. This is due to the link $k_h^* \sim d_h^*$ [see Eq. (8)] and large values of $d_h^* \approx 1000$ pC / N [20]. These values are achieved in the lead-containing composites listed in Table 5 and are about five times larger than d_h^* = 189 pC / N at $\max k_h^*$ in the studied KNNTL:Mn-based composite wherein the aspect ratio of the SC inclusions in ρ_i = 100.

Finally, our comparison of values of the ECF $k_t^* = e_{33}^* / (c_{33}^{*D} \varepsilon_{33}^{*\xi})^{1/2}$ related to the thickness oscillation mode [24] of the 2–0–2 PZT-based [22] and KNNTL:Mn-based composites enables us to state the following

observation. The k_t^* values predicted for the lead-free composite at the volume fractions m and m_i, which are shown in Table 5, are about 15–20% larger than the experimental k_t^* values [22]. Such an advantage is achieved mainly due to the large ECFs of the [001]-poled KNNTL:Mn SC: it is characterised, for instance, by the ECFs k_{33} = 0.95 and k_t = 0.49 [17]. These parameters also make this lead-free SC component competitive among many ferroelectric ceramics [12, 29] and attractive among potential components of novel piezo-active composites.

5. Conclusions

We have studied single crystal (SC) based 2–0–2 composites, whose structure is shown in Fig. 1, and described the effective parameters of these composites [see Eqs. (5)–(8)] and condition (15) to achieve a large piezoelectric anisotropy. The 2–0–2 composite consists of lead-free components, and the primary component providing the piezoelectric activity and sensitivity is the [001]-poled ferroelectric SC (see compositions and constants in Table 1). The second piezoelectric component is the $Li_2B_4O_7$ (LBO) SC that is represented as a system of inclusions aligned in the polymer matrix (Type II layer, 0–3 composite). On varying the volume fractions m and m_i of the first and second SC components and the aspect ratio ρ_i of the SC inclusions in the Type II layer, we find maxima of the parameters from Eqs. (5)–(8) and examine the validity of the condition (15).

The following items are to be emphasised. First, we have used components with contrasting properties: for instance, (i) domain-engineered SC with a relatively high piezoelectric activity (see Table 1), (ii) piezoelectric SC with a low piezoelectric activity and a unique anisotropy of elastic properties (see Table 2), and (iii) piezo-passive isotropic polymer. Second, both the SC components are from the 4*mm* symmetry class, and this circumstance facilitates the further analysis of the effective properties of the composite. Third, the piezoelectric activity of the Type I layer and the active role of the elastic properties of the Type II layer lead to large hydrostatic parameters in specific ranges of the volume fractions m and m_i and aspect ratios ρ_i; see data in Figs. 2–4 and Table 4. Maximum values of the hydrostatic parameters of the 2–0–2 KNNTL:Mn-based composite are 2–6 times larger than the related parameters of the nanostructured [14] and textured [33] ceramic materials with improved piezoelectric properties. Fourth, due to the correlation between $(Q_h^*)^2$ and k_h^* in the presence of the anisotropic Type II layers, it is possible to select volume-fraction (m) ranges wherein maxima or large values of these effective parameters are predicted. Fifth, the large piezoelectric anisotropy of the 2–0–2 composite is caused by the elastic anisotropy of the Type II layer, especially at the aspect ratio $\rho_i >> 1$; see Table 3. Sixth, the sign-variable behaviour of the elastic compliance $s_{12}^{(2),E}$ of the Type II layer is of interest due to the correlation between the location of the absolute max k_h^* and the point where equality $s_{12}^{(2),E} = 0$ holds; see Fig. 4a. To the best of our knowledge, no similar correlation was earlier mentioned in papers on the piezo-active composites.

In general, sets of large values of the studied hydrostatic parameters (Figs. 2–3) and the large piezoelectric anisotropy (Fig. 5) are not typical of the two- or three-component composites [3, 4, 6, 7] based on lead-containing relaxor-ferroelectric SCs and were not mentioned in work [22] on the 2–0–2 PZT ceramic-based composite. Undoubtedly, the characteristics of the novel lead-free 2–0–2 composites make these materials attractive for hydroacoustic, piezoelectric sensor and energy-harvesting applications with due respect to the environment.

Acknowledgements

The authors would like to thank Prof. Dr. A. E. Panich, Prof. Dr. I. A. Parinov, and Prof. Dr. A. A. Nesterov (Southern Federal University, Rostov-on-Don, Russia), and Prof. Dr. S.-H. Chang (National Kaohsiung Marine University, Taiwan, ROC) for their continuing interest in the research problems. Prof. Dr. C. R. Bowen would like to acknowledge funding from the European Research Council under the European Union's Seventh Framework Programme (FP/2007-2013) / ERC Grant Agreement no. 320963 on Novel Energy Materials, Engineering Science and Integrated Systems (NEMESIS). In the present paper, the results on the research project No. 11.1627.2017/4.6 PCh have been represented within the framework of the state task in the scientific activity area at the Southern Federal University, and Prof. Dr. V. Yu. Topolov acknowledges funding with thanks. This research has been performed using the equipment of the Centre of Collective Use ‘High Technologies’ at the Southern Federal University.

References

[1] K. Ren, Y. Liu, X. Geng, H. F. Hofmann, Q. M. Zhang, Single crystal PMN-PT/epoxy 1–3 composite for energy-harvesting application, IEEE Trans. Ultrason. Ferroelectr., a. Freq. Control 53 (2006) 631–638.

[2] F. Wang, C. He, Y. Tang, X. Zhao, H. Luo, Single-crystal $0.7Pb(Mg_{1/3}Nb_{2/3})O_3– 0.3PbTiO_3$ / epoxy 1–3 piezoelectric composites prepared by the lamination technique, Mater. Chem. Phys. 105 (2007) 273–277.

[3] C. R. Bowen, V. Yu. Topolov, A. N. Isaeva, P. Bisegna, Advanced composites based on relaxor-ferroelectric single crystals: from electromechanical coupling to energy-harvesting applications, CrystEngComm 18 (2016) 5986–6001.

[4] C. R. Bowen, V. Yu. Topolov, H. A. Kim, Modern Piezoelectric Energy-harvesting Materials, Springer, Switzerland, 2016.

[5] K. C. Cheng, H. L. W. Chan, C. L. Choy, Q. Yin, H. Luo, Z. Yin, Single crystal PMN– 0.33PT / epoxy 1–3 composites for ultrasonic transducer applications, IEEE Trans. Ultrason., Ferroelec., a. Freq. Contr., 2003, 50, 1177–1183.

[6] S. Zhang F. Li, High performance ferroelectric relaxor-$PbTiO_3$ single crystals: Status and perspective, J. Appl. Phys. 111 (2012) 031301.

[7] S. Zhang, F. Li, J. Luo, R. Sahul, T. R. Shrout, Relaxor-$PbTiO_3$ single crystals for various applications, IEEE Trans. Ultrason., Ferroelec., a. Freq. Contr., 2013, 60 (2013) 1572–1580.

[8] A. Safari, M. Hejazi, Lead-free Piezoelectrics, Eds. S. Priya, and S. Nahm (Springer, New York, Dordrecht, Heidelberg, London, 2012), 139.

[9] A. Ando, Alkali niobate piezoelectric ceramics, in: S. Priya, S. Nahm (eds.), Lead-free Piezoelectrics, Springer, New York, Dordrecht, Heidelberg, London, 2012, pp, 177–208.

[10] C.-H. Hong, H.-P. Kim, B.-Y. Ghoi, H.-S. Han, J.-S. Son, C. W. Ahn, W. Jo, Lead-free piezoceramics – Where to move on? J. Materiomics 2 (2016) 1–24.

[11] I. Coondoo, N. Panwar, A. Kholkin, Lead-free piezoelectrics: Current status and perspectives, J. Adv. Dielectr. 3 (2013) 1330002.

[12] Y. Xu, Ferroelectric Materials and Their Applications, North-Holland, Amsterdam, London, New York, Toronto, 1991.

[13] K. Uchino, Applications of lead-free piezoelectrics, in: S. Priya, S. Nahm (eds.), Lead-free Piezoelectrics, Springer, New York, Dordrecht, Heidelberg, London, 2012, pp, 511–528.

[14] L. G. Gusakova, V. M. Poguibko, N. A. Spiridonov, V. M. Ishchuk, N. K. Kisel', Lead-free nanostructured piezoceramic material based on (K, Na)NbO_3, Nanosystems, Nanomaterials, Nanotechnologies 10 (2012) 303–312 (in Russian).

[15] L. M. Zheng, X. Q. Huo, R. Wang, J. J. Wang, W. H. Jiang, W. W. Cao, Large size lead-free (Na, K)(Nb, Ta)O_3 piezoelectric single crystal: growth and full tensor properties, CrystEngComm, 15 (2013) 7718–7722.

[16] X. Huo, L. Zheng, R. Zhang, R. Wang, J. Wang, S. Sang, Y. Wang, B. Yang, W. Cao, High quality lead-free (Li, Ta) modified (K, Na)NbO_3 single crystal and its complete set of elastic, dielectric and piezoelectric coefficients with macroscopic 4mm symmetry, CrystEngComm 16 (2014) 9828–9833.

[17] X. Huo, R. Zhang, L. Zheng, S. Zhang, R. Wang, J. Wang, S. Sang, B. Yang, W. Cao, (K, Na, Li)(Nb, Ta)O_3:Mn lead-free single crystal with high piezoelectric properties, J. Am. Cer. Soc. 98 (2015) 1829–1835.

[18] V. Yu. Topolov, C. R. Bowen, High-performance 1–3-type lead-free piezo-composites with auxetic polyethylene matrices, Mater. Lett. 142 (2015) 265–268.

[19] V. Yu. Topolov, C. R. Bowen, F. Levassort, Piezoelectric sensitivity and anisotropy of a novel lead-free 2–2 composite, in: I.A. Parinov, S.-H. Chang, V. Yu. Topolov (eds.), Proceedings of the 2015 International Conference on "Physics, Mechanics of New Materials and Their Applications", Devoted to the 100th Anniversary of the Southern Federal University, Nova Sci. Publ., New York, 2016, pp. 131–139.

[20] V. Yu. Topolov, C. R. Bowen, I. A. Ermakov, Remarkable hydrostatic piezoelectric response of novel 2–0–2 composites, Ferroelectrics. Lett. Sec. 43 (2016) 90–95.

[21] R. E. Newnham, D. P. Skinner, L. E. Cross, Connectivity and piezoelectric-pyroelectric composites, Mater. Res. Bull. 13 (1978) 525–536.

[22] X. Dongyu, C. Xin, H. Shifeng, Investigation of inorganic fillers on properties of 2–2 connectivity cement / polymer based piezoelectric composites, Constr. Build. Mater. 94 (2015) 678–683.

[23] J. H. Huang, W.-S. Kuo, Micromechanics determination of the effective properties of piezoelectric composites containing spatially oriented short fibers, Acta Mater. 44 (1996) 4889–4898.

[24] T. Ikeda, Fundamentals of Piezoelectricity, Oxford University Press, Oxford, New York, Toronto, 1990.

[25] M. Adachi, T. Shiosaki, H. Kobayashi, O. Ohnishi, A. Kawabata, Temperature compensated piezoelectric lithium tetraborate crystal for high frequency surface acoustic wave and bulk wave device

applications, in: Proceedings of 1985 IEEE Ultrasonics Symposium, IEEE, New York, 1985, pp. 228–232.

[26] L. V. Gibiansky, S. Torquato, On the use of homogenization theory to design optimal piezocomposites for hydrophone applications, J. Mech. Phys. Solids 45 (1997), 689–708.

[27] K. E. Evans, K. L. Alderson, The static and dynamic moduli of auxetic microporous polyethylene, J. Mater. Sci. Lett. 11 (1992) 1721–1724.

[28] I. N. Groznov, Dielectric permittivity, in: Physics Encyclopaedia, Sovetskaya Entsiklopediya, Moscow, 1983 (in Russian), p. 178–179.

[29] S. Ikegami, I. Ueda, T. Nagata, Electromechanical properties of $PbTiO_3$ ceramics containing La and Mn, J. Acoust. Soc. Am. 50 (1971) 1060–1066.

[30] R. Zhang, B. Jiang, W. Cao, Elastic, piezoelectric, and dielectric properties of multidomain $0.67Pb(Mg_{1/3}Nb_{2/3})O_3$–$0.33PbTiO_3$ single crystals, J. Appl. Phys. 90 (2001) 3471–3475.

[31] A. A. Grekov, S. O. Kramarov, A. A. Kuprienko, Anomalous behavior of the two-phase lamellar piezoelectric texture, Ferroelectrics 76 (1987) 43–48.

[32] C. R. Bowen, D. N. Betts, H. A. Kim, V. Yu. Topolov, 2–2 composites based on [011]-poled relaxor-ferroelectric single crystals: analysis of the piezoelectric anisotropy and squared figures of merit for energy harvesting applications, Microsyst. Technol. 20 (2014) 709–717.

[33] Y. Yan, J. E. Zhou, D. Maurya, Y. U. Wang, S. Priya, Giant piezoelectric voltage coefficient in grain-oriented modified $PbTiO_3$ material, Nature Communs 7 (2016) 13089.

[34] R. Rouffaud, P. Marchet, A.-C. Hladky-Hennion, C. Bantignies, M. Pham-Thi, F. Levassort, Complete electroelastic set for the (YXt)-45° cut of a $KNbO_3$ single crystal, J. Appl. Phys. 116 (2014) 194106.

[35] E. K. Akdogan, M. Allahverdi, A. Safari, Piezoelectric composites for sensor and actuator applications, IEEE Trans. Ultrason., Ferroelec., a. Freq. Contr. 52 (2005) 746–775.

To the paper "Piezoelectric sensitivity and hydrostatic response of novel lead-free 2–0–2 composites with two single-crystal components" by V. Yu. Topolov et al.

Table 1. Room-temperature elastic compliances s_{ab}^E (in 10^{-12} Pa^{-1}), piezoelectric coefficients d_{ij} (in pC / N) and dielectric permittivity $\varepsilon_{pp}^{\sigma}$ of the [001]-poled domain-engineered SC[a] components

Components	s_{11}^E	s_{12}^E	s_{13}^E	s_{33}^E	s_{44}^E	s_{66}^E	d_{31}	d_{33}	d_{15}	$\varepsilon_{11}^{\sigma}/\varepsilon_0$	$\varepsilon_{33}^{\sigma}/\varepsilon_0$
KNN–T[b]	11.9	–4.30	–5.60	15.5	12.0	10.7	–77.0	162	45.0	291	267
KNN–TL[c]	17.2	–5.11	–10.7	27.0	15.4	13.9	–163	354	171	1100	790
KNNTL:Mn[d]	33.4	–7.36	–25.8	57.7	12.8	13.5	–260	545	66	400	650

[a] Data are related to the main crystallographic axes of the SC with macroscopic 4*mm* symmetry

[b] $(K_{0.562}Na_{0.438})(Nb_{0.768}Ta_{0.232})O_3$, Ref. 15

[c] $[Li_x(K_{0.501}Na_{0.499})_{1-x}](Nb_{0.660}Ta_{0.340})O_3$, Ref. 16

[d] $[Li_x(K_{1-y}Na_y)_{1-x}](Nb_{1-z}Ta_z)O_3$:Mn, where $x = 0.06$, $y = 0.1$–0.3, $z = 0.07$–0.17, and the level of Mn doping is 0.25 mol. %, Ref. 17

Table 2. Room-temperature elastic moduli c_{ab} (in 10^{10} Pa), piezoelectric coefficients e_{ij} (in C / m^2) and dielectric permittivity ε_{pp} of SC and polymer components in the Type II layer

Components	c_{11}^E	c_{12}^E	c_{13}^E	c_{33}^E	c_{44}^E	c_{66}^E	e_{31}	e_{33}	e_{15}	$\varepsilon_{11}^{\xi}/\varepsilon_0$	$\varepsilon_{33}^{\xi}/\varepsilon_0$
LBO SC[a]	13.5	0.357	3.35	5.68	5.85	4.67	0.290	0.928	0.472	8.90	8.07
Polyurethane[b]	0.442	0.260	0.260	0.442	0.091	0.091	0	0	0	3.5	3.5
PE[c]	0.0778	0.0195	0.0195	0.0778	0.0292	0.0292	0	0	0	2.3	2.3

[a] 4*mm* symmetry, the full set of electromechanical constants is taken from Ref. 25

[b] Ref. 26

[c] Elastic and dielectric properties are taken from Ref. 27 and Ref. 28, respectively

Table 3. Aspect-ratio dependence of elastic compliances $s_{ab}^{(2),E}$ (in 10^{-12} Pa^{-1}) of the 0–3 LBO SC / PE composite at m_i = const

ρ_i	$s_{11}^{(2),E}$	$s_{12}^{(2),E}$	$s_{13}^{(2),E}$	$s_{33}^{(2),E}$	$s_{11}^{(2),E}$	$s_{12}^{(2),E}$	$s_{13}^{(2),E}$	$s_{33}^{(2),E}$
	At m_i = 0.10				At m_i = 0.20			
0.01	123	–26.0	–19.9	96.5	106	–22.7	–15.5	72.9
0.1	122	–24.8	–20.5	97.3	104	–20.9	–16.2	73.7
0.5	117	–20.7	–24.7	108	96.4	–15.0	–21.4	85.9
1	112	–18.7	–26.5	118	88.5	–12.4	–23.9	98.5
1.5	106	–17.4	–26.5	122	82.0	–10.9	–23.9	105
2	102	–16.1	–26.0	125	76.6	–9.60	–23.3	108
3	95.1	–13.9	–24.8	127	68.7	–7.56	–21.6	112
5	85.7	–10.7	–22.8	128	59.2	–4.86	–19.2	113
10	74.4	–6.50	–20.2	128	49.1	–1.84	–16.2	114
50	59.9	–1.08	–16.8	126	38.0	1.38	–12.6	113
100	57.6	–0.218	–16.2	126	36.3	1.83	–12.0	113

Table 4. Data on local maxima of squared figures of merit $(Q_{33}^*)^2$ and $(Q_h^*)^2$ (in 10^{-12} Pa^{-1}) and ECF k_h^* of 2–0–2 PE-containing composites at $\rho_i = 100$ and m_i = const. The volume fraction m related to the maximum value is given in parentheses

max[$(Q_{33}^*)^2$]	max[$(Q_h^*)^2$]	max k_h^*	max[$(Q_{33}^*)^2$]	max[$(Q_h^*)^2$]	max k_h^*
KNN–T SC / LBO SC / PE composite					
At m_i = 0.05			At m_i = 0.10		
168 (0.022)	72.4 (0.016)	0.303 (0.024)	153 (0.022)	83.8 (0.017)	0.375 (0.029)
At m_i = 0.30			At m_i = 0.50		
116 (0.027)	81.8 (0.022)	0.488 (0.025)	88.7 (0.035)	63.8 (0.030)	0.525 (0.067)
KNN–TL SC / LBO SC / PE composite					
At m_i = 0.05			At m_i = 0.10		
233 (0.021)	112 (0.016)	0.354 (0.025)	210 (0.022)	126 (0.017)	0.425 (0.031)
At m_i = 0.30			At m_i = 0.50		
157 (0.026)	117 (0.022)	0.526 (0.051)	116 (0.035)	88.5 (0.029)	0.555 (0.074)

Table 5. Comparison of hydrostatic parameters of the 2–0–2 composites at $\rho_i = 100$

m_i	m	g_h^*, mV·m / N	k_h^*	g_h^*, mV·m / N	k_h^*	g_h^*, mV·m / N	k_h^*
		KNNTL:Mn SC / LBO SC / PE composite[a]		PMN–0.33PT SC / modified $PbTiO_3$ ceramic / PE composite[b]		PZN–0.08PT SC / modified $PbTiO_3$ ceramic / PE composite[b]	
0.10	0.05	498	0.381	520	0.678	499	0.623
	0.10	335	0.428	255	0.650	257	0.615
	0.15	231	0.422	159	0.610	162	0.584
	0.20	168	0.404	111	0.571	113	0.549
0.20	0.05	529	0.428	543	0.744	514	0.677
	0.10	380	0.504	275	0.741	274	0.695
	0.15	270	0.512	174	0.715	176	0.680
	0.20	199	0.500	122	0.685	124	0.655

[a] From the present study

[b] Studied in work [20]. The aspect ratio $\rho_i = 100$ is related to the ceramic inclusions in the Type II layer (instead of SC-2 shown in the inset 2 of Fig. 1)

Figure captions to the paper "Piezoelectric sensitivity and hydrostatic response of novel lead-free 2–0–2 composites with two single-crystal components"

by V. Yu. Topolov, C. R. Bowen, A. A. Panich, and A. N. Isaeva

Fig. 1. Schematic of the 2–0–2 SC-1 / SC-2 / polymer composite. ($X_1X_2X_3$) is a rectangular co-ordinate system, m and $1 - m$ are volume fractions of the type I and type II layers, respectively, $\boldsymbol{P}_s^{(1)}$ is the spontaneous polarisation vector of the domain-engineered SC-1 poled along the OX_3 axis, m_i is the volume fraction of the SC-2 inclusions in the polymer medium, and a_1 and a_3 are semi-axes of each inclusion.

Fig. 2. Aspect-ratio (ρ_i) dependences of piezoelectric coefficients g_{31}^* (a, in mV·m / N), g_{32}^* (b, in mV·m / N) and g_{33}^* (c, in mV·m / N), squared figure of merit $(Q_{33}^*)^2$ (d, in 10^{-12} Pa^{-1}), and hydrostatic piezoelectric coefficient g_h^* (e, in mV·m / N), squared figure of merit $(Q_h^*)^2$ (f, in 10^{-12} Pa^{-1}) and ECF k_h^* (g) of the 2–0–2 KNNTL:Mn SC / LBO SC / PE composite at $m_i = 0.10$.

Fig. 3. Volume fraction (m and m_i) dependences of the piezoelectric coefficient g_{33}^* (a and e, in mV·m / N) and hydrostatic piezoelectric coefficient g_h^* (b, in mV·m / N), squared figure of merit $(Q_h^*)^2$ (c, in 10^{-12} Pa^{-1}) and ECF k_h^* (d and f) of the 2–0–2 KNNTL:Mn SC / LBO SC / PE (a–d) and KNNTL:Mn SC / LBO SC / polyurethane (e and f) composites at $\rho_i = 100$.

Fig. 4. Behaviour of effective parameters of the 2–0–2 KNNTL:Mn SC / LBO SC / PE composite near its max k_h^* at $\rho_i = 100$: (a) link between the local maximum of the ECF $(k_h^*)_m$ and the elastic compliance $s_{12}^{(2),E}$ (in 10^{-12} Pa^{-1}) of the Type II layer, (b) optimal volume fraction m_{maxkh} of SC-1, and (c) volume-fraction (m_i) dependences of the elastic compliance s_{12}^{*E} (in 10^{-12} Pa^{-1}), piezoelectric coefficient d_h^* (in pC / N) and dielectric permittivity $\varepsilon_{33}^{*\sigma}$ of the aforementioned 2–0–2 composite.

Fig. 5. Volume-fraction (m) region related to the large anisotropy of the piezoelectric coefficients g_{3j}^* at $0.05 \le m_i \le 0.75$ and $\rho_i = 100$. Calculations were performed for the 2–0–2 KNNTL:Mn SC / LBO SC / PE composite. The shaded region is related to the valid condition (15).

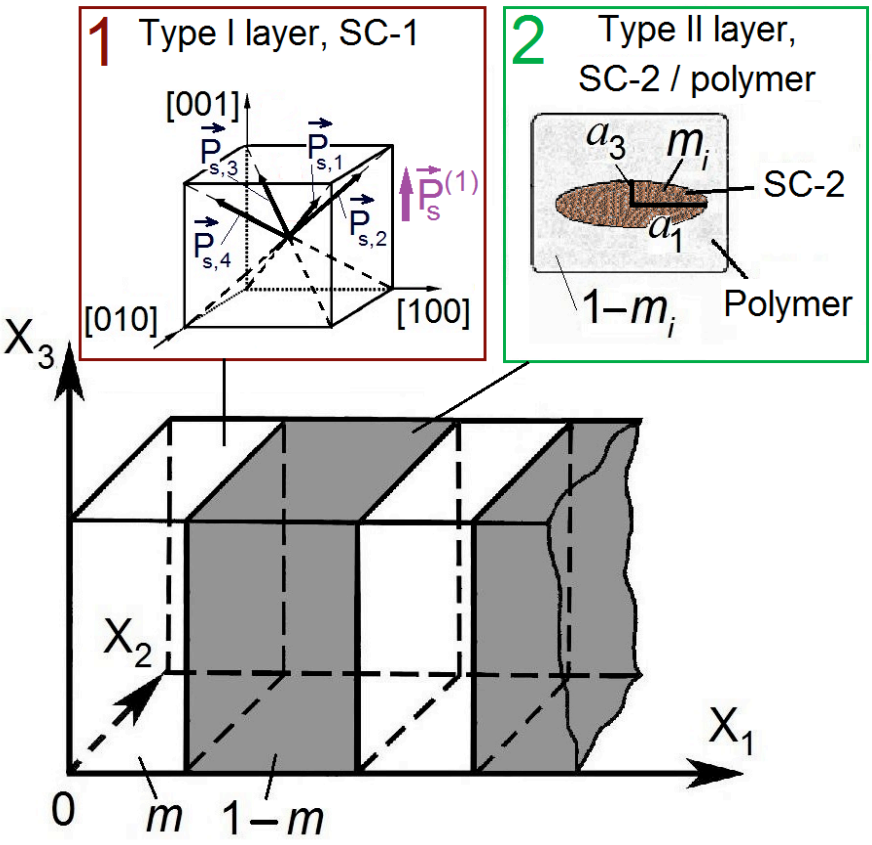
1
Type I layer, SC-1
[001]
[010]
[100]
2
Type II layer,
SC-2 / polymer
SC-2
Polymer
X3
X2
X1
0
m
1 – m

Fig. 1

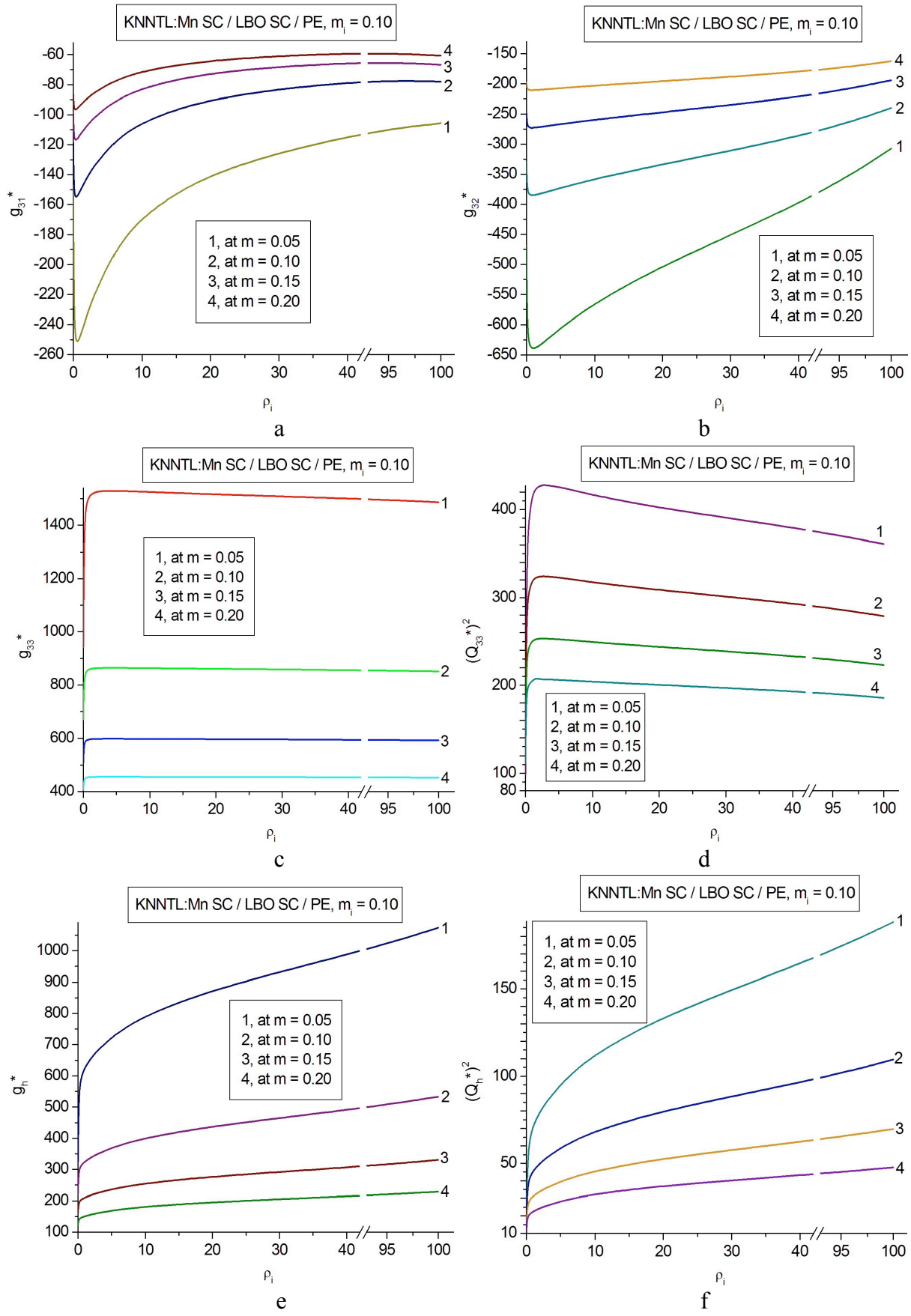

Fig. 2 (*continued*)

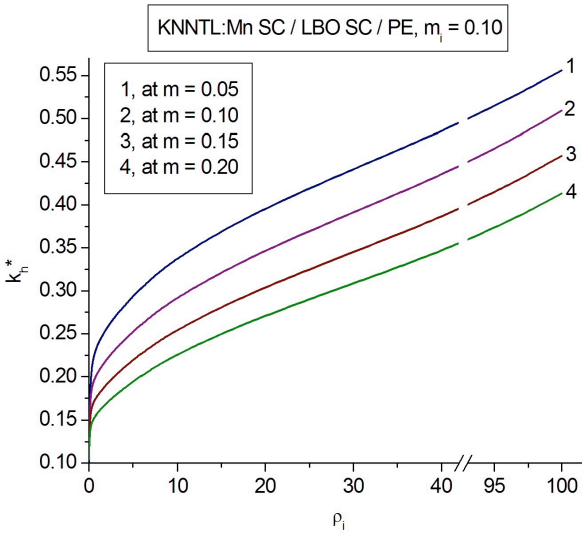
KNNTL:Mn SC / LBO SC / PE, m_i = 0.10
1, at m = 0.05
2, at m = 0.10
3, at m = 0.15
4, at m = 0.20
k_h*
ρ_i
0.55
0.50
0.45
0.40
0.35
0.30
0.25
0.20
0.15
0.10
0
10
20
30
40
95
100
1
2
3
4

g

Fig. 2

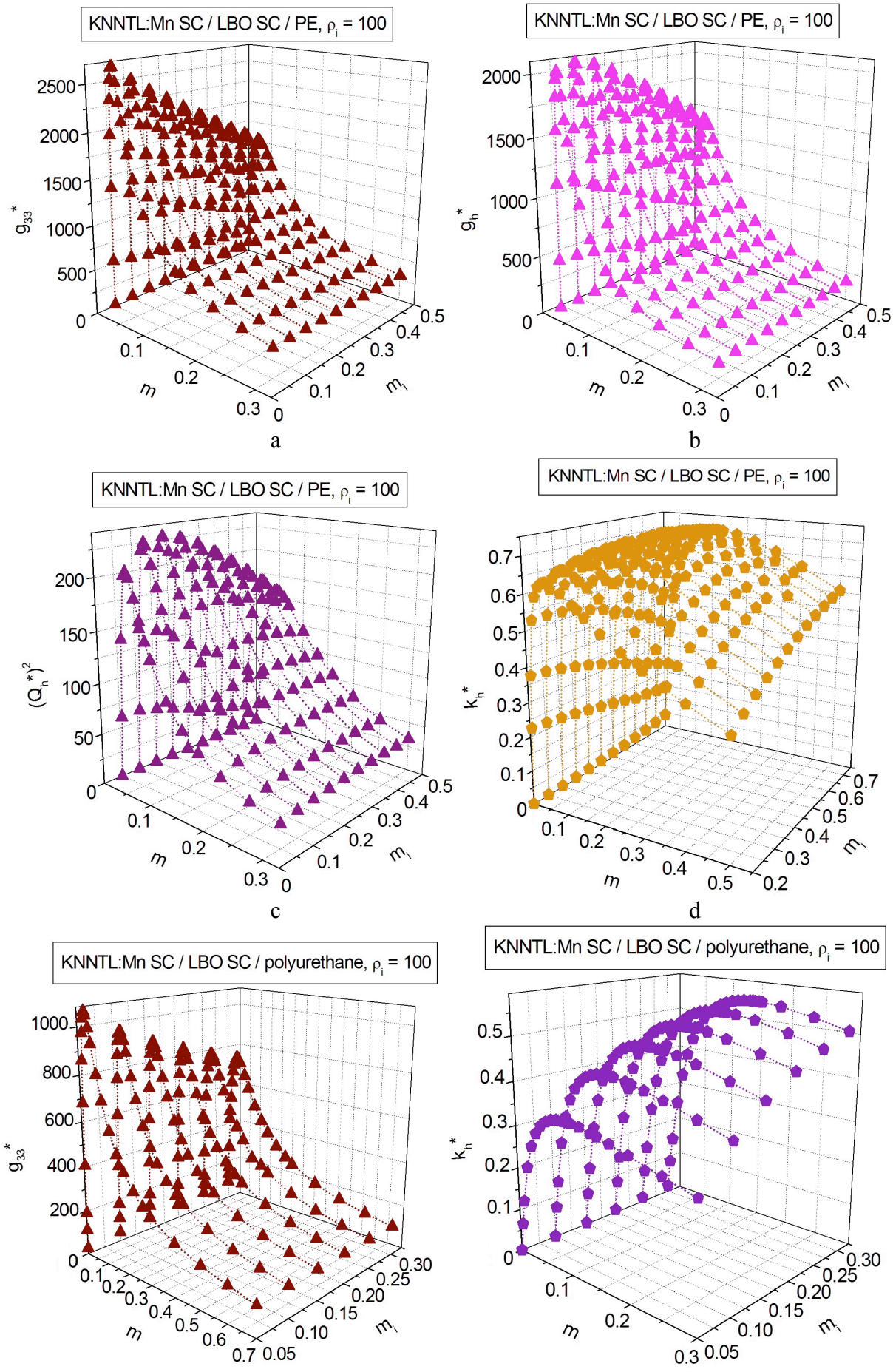
KNNTL:Mn SC / LBO SC / PE, ρi = 100
g33*
m
mi
a
KNNTL:Mn SC / LBO SC / PE, ρi = 100
gh*
m
mi
b
KNNTL:Mn SC / LBO SC / PE, ρi = 100
(Qh*)2
m
mi
c
KNNTL:Mn SC / LBO SC / PE, ρi = 100
kh*
m
mi
d
KNNTL:Mn SC / LBO SC / polyurethane, ρi = 100
g33*
m
mi
e
KNNTL:Mn SC / LBO SC / polyurethane, ρi = 100
kh*
m
mi
f

Fig. 3

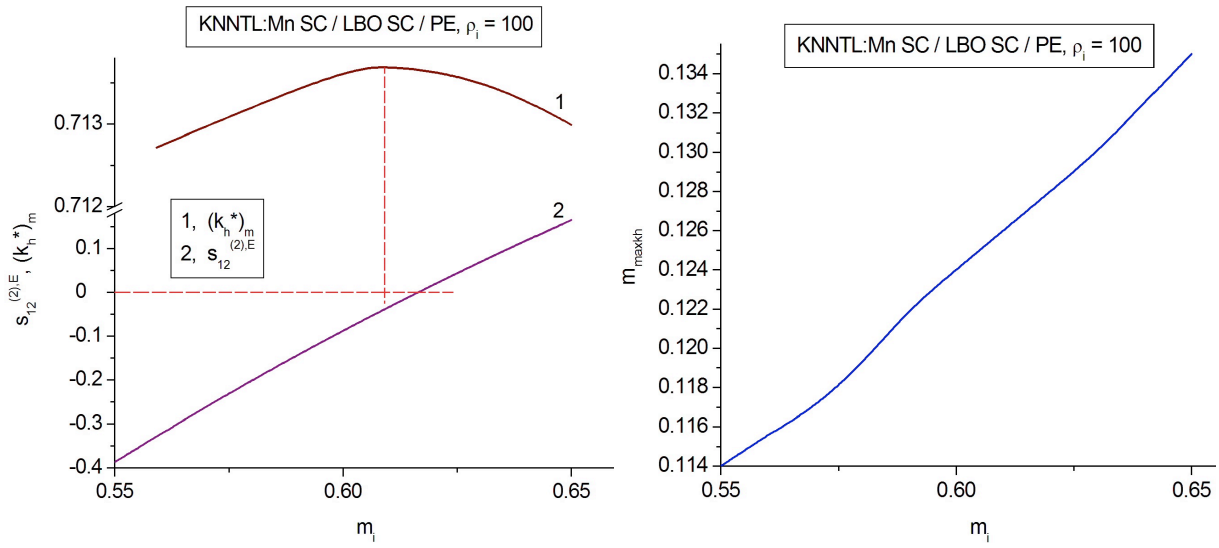
KNNTL:Mn SC / LBO SC / PE, ρi = 100
1, (kh*)m
2, s12(2),E
s12(2),E , (kh*)m
mi
a
KNNTL:Mn SC / LBO SC / PE, ρi = 100
mmaxkh
mi
b

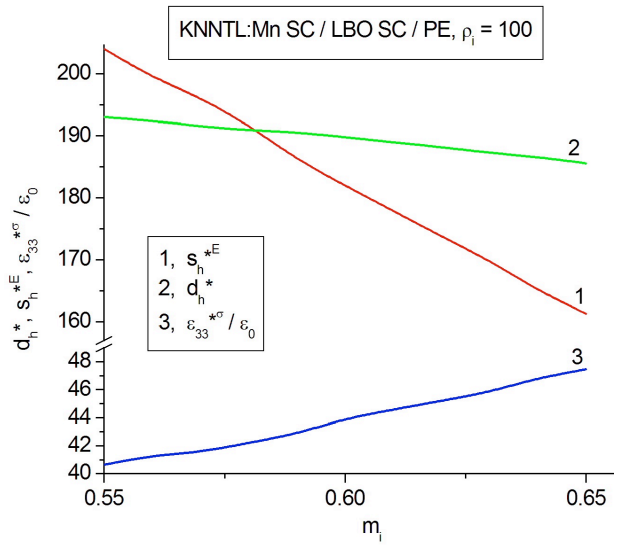
KNNTL:Mn SC / LBO SC / PE, ρi = 100
1, sh*E
2, dh*
3, ε33*σ / ε0
dh* , sh*E , ε33*σ / ε0
mi
c

Fig. 4

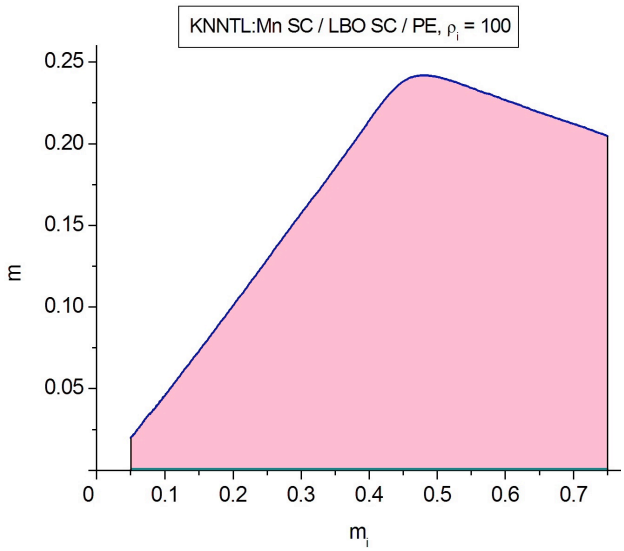
KNNTL:Mn SC / LBO SC / PE, ρi = 100
m
mi

Fig. 5